Supporting Information (SI)

Materials

Carbon black (CB, Alfa Aesar (China) Chemical Co., Ltd.), 1H, 1H, 2H, 2H-Perfluorodecyltriethoxysilane (FAS, Aladdin Shanghai, Aladdin Biochemical Technology Co., Ltd.), polyvinylidene fluoride PVDF (Zhanyang Polymer Materials). Sulfuric acid (H_2SO_4), N, N-dimethylformamide (DMF), Sodium chloride (NaCl), magnesium chloride hexahydrate ($MgCl_2 \cdot 6H_2O$), potassium chloride (KCl), calcium chloride ($CaCl_2$), sodium sulfate (Na_2SO_4), sodium bicarbonate ($NaHCO_3$,) and potassium bromide (KBr) from Kermel, Tianjin Kermel Chemical Reagent Co., Ltd. Pre-treatment of waste masks were performed to remove large particles via the washing by ethanol for 30 min under ultrasound and annealing at 60 °C for 20 min.

Preparation of PP-OCB-PVDF

10 mg/mL of PVDF solution in DMF was prepared. After stirring the PVDF solution for 1 h, 10 mg/mL of OCB nanoparticles were added and kept stirring for 3 h to obtain the coating solution. The prepared OCB-PVDF coating solution was coated on the cleaned PP-waste mask using painting brush and dried at 100 °C for 1 h.

Preparation of PP-HCB

10 mg/mL of HCB nanoparticles were dispersed in DMF and stirred for 3 h. Then, the HCB suspension was coated on the surface of the cleaned mask and dried at 100 °C for 1 h to obtain PP-HCB.

Characterizations

The scanning electron microscopy (SEM, JSM-7610F, JEOL Ltd., Japan) was used to characterize the surface morphology of coatings. The elemental content and chemical interaction of coating composites on the surface were studied by energy dispersive spectroscopy (EDS, JSM-7610F, Japan) and X-ray photoelectron microscopy (XPS, D8 Advance, Bruker, Germany details of instruments), respectively. The contact angle of

coatings was measured with a goniometer. The water contact angle (WCA) of the sample surface was determined using a contact angle measurement angle measurement unit (SCI6000E, POWEREACH, China China) using with a 4 μL water droplet. The absorption and reflection spectra of coatings were determined by UV/vis spectroscopy (UV-3600UH5700; Shimadzu, HITACHI, Japan). Infrared images and the temperature change of samples were procured by an infrared thermal imager (FLIR E8xtFLIR T440, USA). The interfacial solar vapor generation and water desalination was carried out on a lab-made setup. The solar radiations were generated during the procreated using experiment using a solar simulator (CELS500L, AULTT, China).

Solar-driven seawater desalination experiment

The water evaporator unit is placed under a Xenon lamp (CELS500L) fitted with a Xenon lamp for the water evaporation test. The change in mass of the water during evaporation was recorded by an electronic balance. The evaporation rate of water based on the same photothermal material under dark conditions (0.074 $kg \cdot m^{-2} \cdot h^{-1}$) was also tested. And the evaporation rate of water ($m \cdot kg \cdot m^{-2} \cdot h^{-1}$) was obtained from equation (1):

$$m = dm/S \cdot t \qquad (1)$$

where dm is the weight loss of water, S is the evaporation area of the water evaporator unit and t is the evaporation time. And the evaporation efficiency (η) is calculated by equation (2):

$$\eta = \dot{m} h_{LV}/Pin \qquad (2)$$

where $\dot{m}$ is the evaporation rate of the water evaporator unit after subtracting the evaporation rate of the water, h_{Lv} is the enthalpy of phase change of water from liquid to vapor (2256 $J \cdot g^{-1}$) and Pin is the solar illumination intensity.

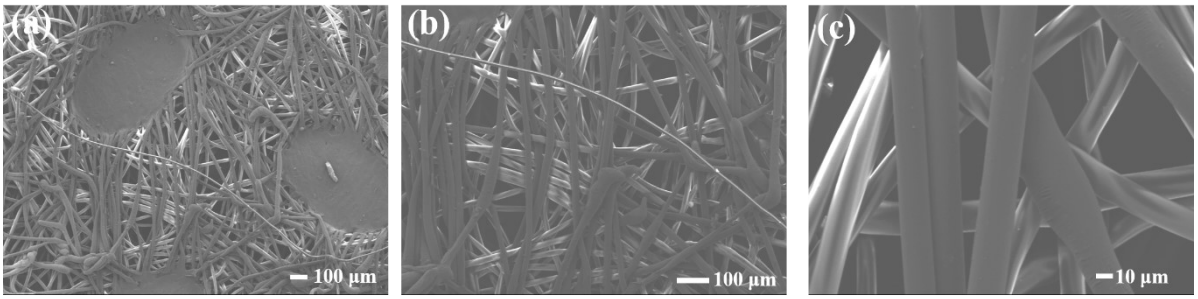

Fig. S1: (a-c) Different magnified SEM images of the original PP-mask.

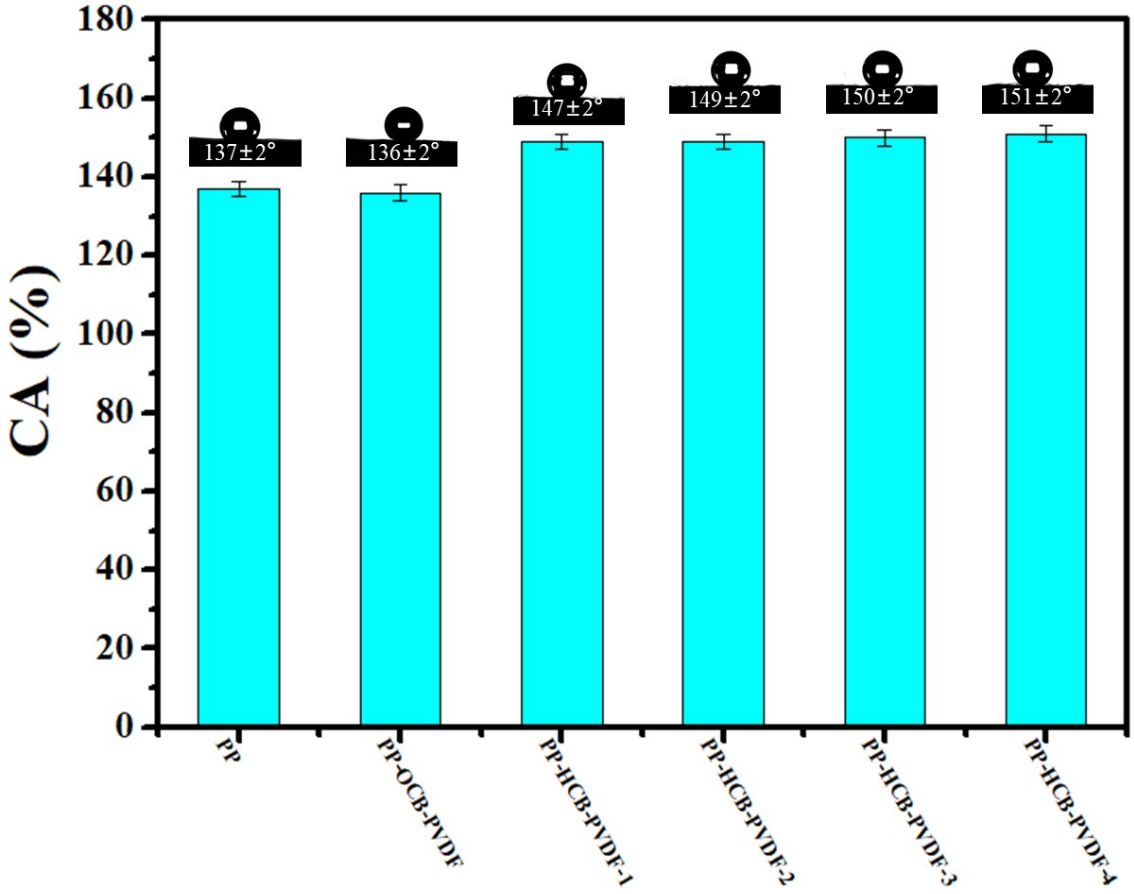

Fig. S2: Variation of water contact angle with respect to samples.

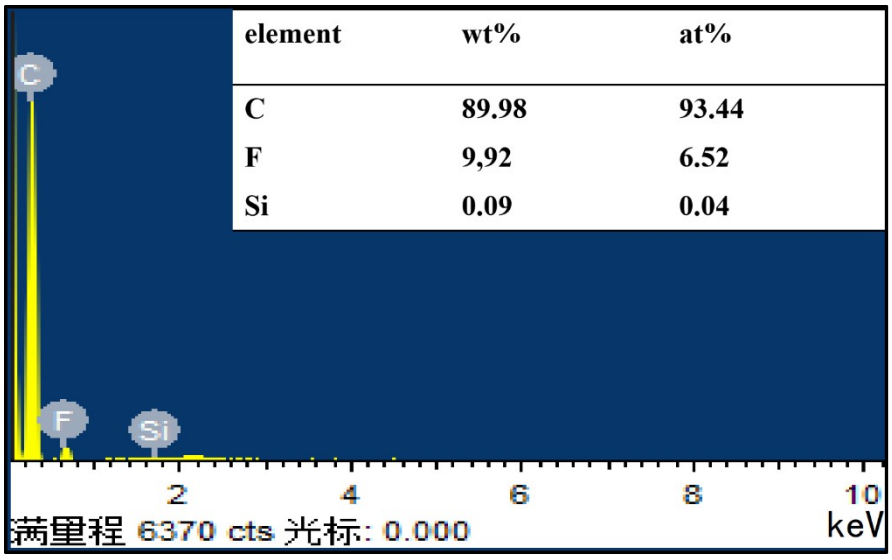

Fig. S3: Mass and atomic percentage of C, F, and Si elements of PP- HCB-PVDF-1 sample.

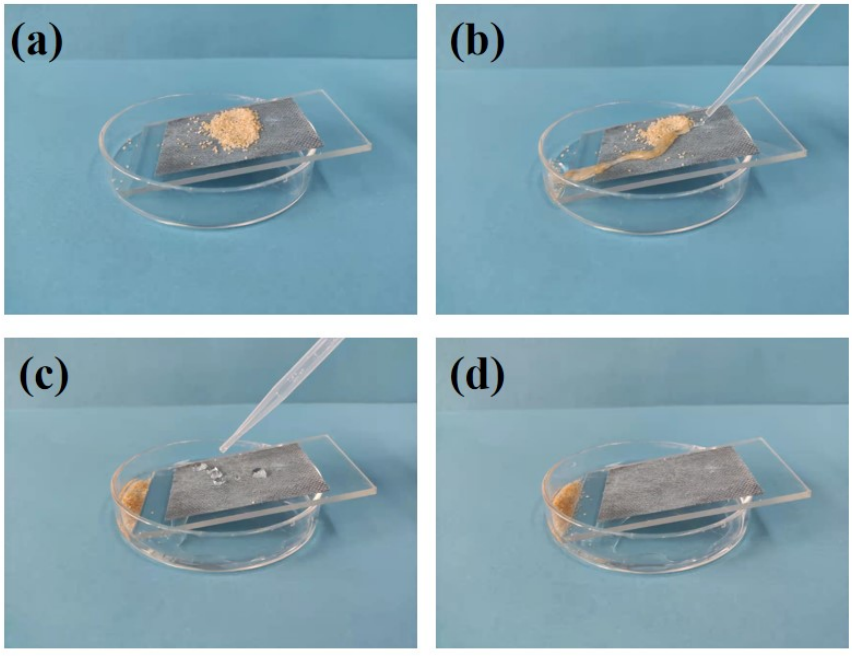

Fig. S4: (a-b) Self-cleaning ability of superhydrophobic photothermal PP-HCB-PVDF-1 surface.

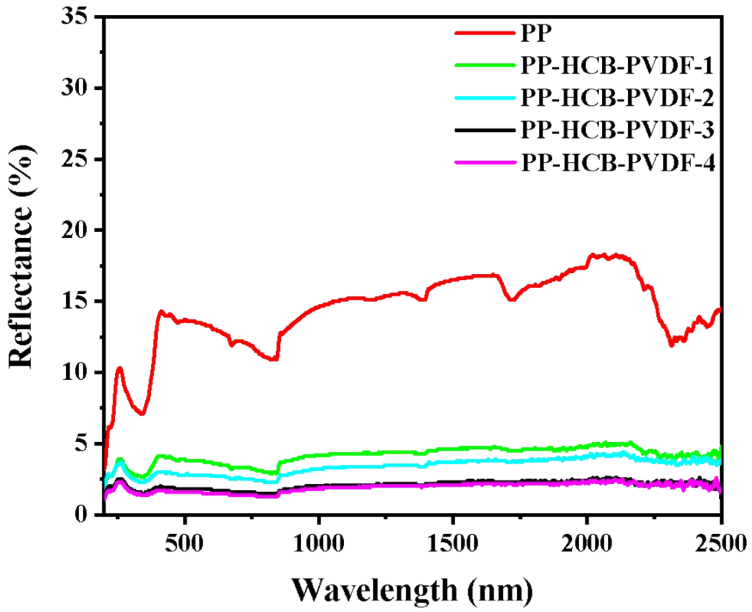

Fig. S5: Reflection spectra of PP and PP-HCB-PVDF-series

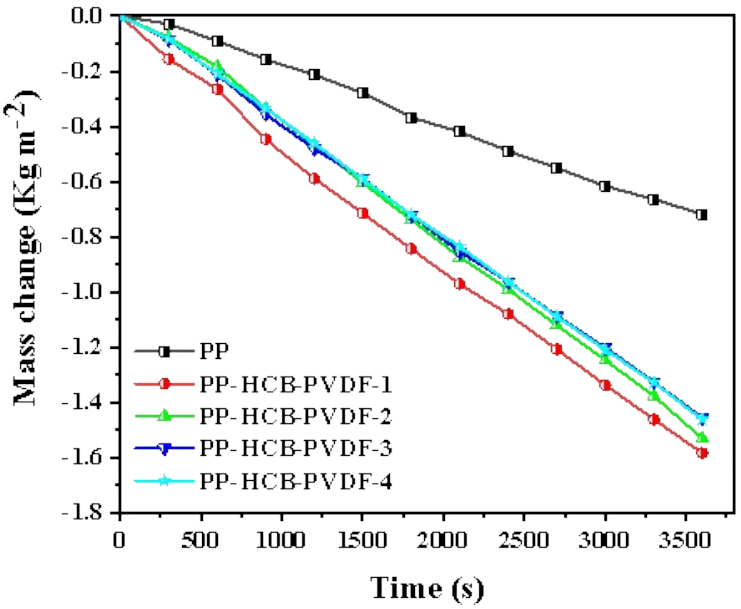

Fig. S6: Mass change during illumination against time response curve of PP-mask and PP-HCB-PVDF samples.

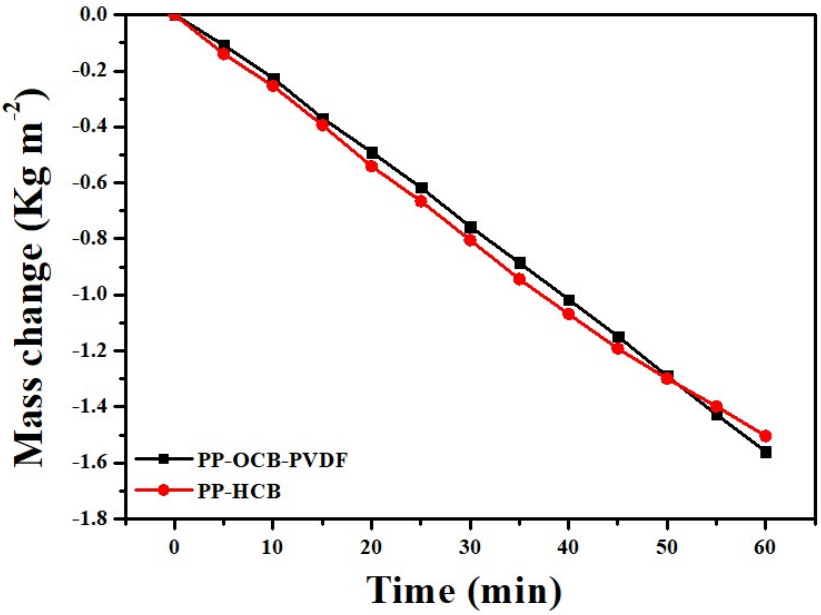

Fig. S7: Mass change during illumination against time response curve of PP-OCB-PVDF and PP-HCB samples.

Table S1 Basic cost of 1m^2 photothermal layer ($)

CB	PVDF	FAS	DMF	H_2SO_4	Total cost
0.35	0.13	1.27	0.11	0.11	1.97

Table S2: The compare study of current research on photothermal evaporator for seawater desalination.

Material	Substrate	Power density [W m^{-2}]	Solution	Evaporation rate kg/(m^2 · h)	Conversion efficiency (%)	Surface wettability	Continuous salt-rejecting	Refence
CB/PVDF	PP	1	3.5 wt % of NaCl solution	1.58	94.3	superhydrophobic	Five cycles, a total of 40 hours	The work
CB/celluose acetate	PVDF membrane	1	35 g/L of NaCl solution	/	75.4	Omniphobic	/	[6]
CB/celluo-se acetate	porous PET	1	water	1.48	98.6	Hydrophilic	6h, simulated Seawater(3-sun)	[5]
La0.7Sr0.3CoO3 slice	/	1	Seawater from Jiaozhou Bay	1.58	92	Superhydrophilic	12h,Seawater (1-sun)	[4]
CuS	PAN fabrics	1	seawater from the Yellow Sea	2.27	/	Superhydrophilic	100 h, seawater (1-sun)	[3]
hierarchically porous graphitic	polyimide foam	1	deionized water	1.34	83.2	hydrophobic	6 h, seawater (1-sun)	[2]
forest-like laser-induced graphene	Polybenzoxazine resin	1	3.5 wt % of NaCl solution	1.25	85.71	superhydrophobic	1)12h, 20wt%NaCl solution, (1-sun)	[1]

Material	Substrate	Power density [W m^{-2}]	Solution	Evaporation raten kg/($m^2 \cdot h$)	Conversion efficiency (%)	Surface wettability	Continuous salt-rejecting	Refence
CuO@PDA/PB	Cu foam	1	water	1.39	87.10	Superhydrophilic	8h, 3.5 wt% NaCl solution,	[13]
PVP and CNTs	expanded polystyrene	1	3.5 wt % of NaCl solution	1.41	91.1	superhydrophobic	40 h,3.5 wt% NaCl solution(1-	[12]
Bi2O3–PMoO SNW	polyethylene foam	1	deionized water	1.38	91.1	hydrophilic	/	[11]
HgSx	synthetic cellulose	1	distilled water	1.30	88.3	hydrophilic	/	[10]
polypyrrole (PPy)	fabric	1	3.6 wt% NaCl solution	1.49	91.68	superhydrophobic	12 h3.6 wt% NaCl solution(1-	[9]
modified hollow glass microspheres (MHGM), conductive carbon	polyimide-based porous membrane and Polyurethane	1	pure water	1.4904	86.65	superhydrophilic	6 h, 15%NaCl (1-sun)	[8]
MnO2	natural paulownia	1	pure water	1.31	81.4	Hydrophilic	6 h10.0 and 20.0 wt % NaCl	[7]

References

[1] Y. Peng, W. Zhao, F. Ni, W. Yu, X. Liu, Forest-like Laser-Induced Graphene Film with Ultrahigh Solar Energy Utilization Efficiency, ACS Nano, 15 (2021) 19490-19502.

[2] M. Kim, K. Yang, Y.S. Kim, J.C. Won, P. Kang, Y.H. Kim, B.G. Kim, Laser-induced photothermal generation of flexible and salt-resistant monolithic bilayer membranes for efficient solar desalination, Carbon, 164 (2020) 349-356.

[3] Z. Liu, Z. Zhou, N. Wu, R. Zhang, B. Zhu, H. Jin, Y. Zhang, M. Zhu, Z. Chen, Hierarchical Photothermal Fabrics with Low Evaporation Enthalpy as Heliotropic Evaporators for Efficient, Continuous, Salt-Free Desalination, ACS Nano, 15 (2021) 13007-13018.

[4] Y. Wang, C. Wang, W. Liang, X. Song, Y. Zhang, M. Huang, H. Jiang, Multifunctional perovskite oxide for efficient solar-driven evaporation and energy-saving regeneration, Nano Energy, 70 (2020) 104538.

[5] R. Zhang, Y. Zhou, B. Xiang, X. Zeng, Y. Luo, X. Meng, S. Tang, Scalable Carbon Black Enhanced Nanofiber Network Films for High‐Efficiency Solar Steam Generation, Advanced Materials Interfaces, 8 (2021) 2101160.

[6] Y.-R. Chen, R. Xin, X. Huang, K. Zuo, K.-L. Tung, Q. Li, Wetting-resistant photothermal nanocomposite membranes for direct solar membrane distillation, Journal of Membrane Science, 620 (2021) 118913.

[7] D. Li, D. Han, C. Guo, C. Huang, Facile Preparation of MnO2-Deposited Wood for High-Efficiency Solar Steam Generation, ACS Applied Energy Materials, 4 (2021) 1752-1762.

[8] S. Wang, Y. Niu, L. Yan, W. Chan, Z. Zhu, H. Sun, J. Li, W. Liang, A. Li, Polyimide-based superhydrophilic porous membrane with enhanced thermal insulation for efficient interfacial solar evaporation, Composites Science and Technology, 228 (2022) 109683.

[9] C. Zhang, P. Xiao, F. Ni, J. Gu, J. Chen, Y. Nie, S.-W. Kuo, T. Chen, Breathable and superhydrophobic photothermic fabric enables efficient interface energy management via confined heating strategy for sustainable seawater evaporation, Chemical Engineering Journal, 428 (2022) 131142.

[10] M. Li, M. Yang, B. Liu, H. Guo, H. Wang, X. Li, L. Wang, T.D. James, Self-assembling

fluorescent hydrogel for highly efficient water purification and photothermal conversion, Chemical Engineering Journal, 431 (2022) 134245.

[11] S. Zhang, Q. Lu, B. Yu, X. Cheng, J. Zhuang, X. Wang, Polyoxometalates Facilitating Synthesis of Subnanometer Nanowires, Advanced Functional Materials, 31 (2021) 2100703.

[12] C. Shen, Y. Zhu, X. Xiao, X. Xu, X. Chen, G. Xu, Economical Salt-Resistant Superhydrophobic Photothermal Membrane for Highly Efficient and Stable Solar Desalination, ACS Applied Materials & Interfaces, 12 (2020) 35142-35151.

[13] R. Zhu, M. Liu, Y. Hou, D. Wang, L. Zhang, D. Wang, S. Fu, Mussel-inspired photothermal synergetic system for clean water production using full-spectrum solar energy, Chemical Engineering Journal, 423 (2021) 129099.